Modelling materials for solar fuel synthesis by artificial photosynthesis; predicting the optical, electronic and redox properties of photocatalysts

Topical Review

Modelling materials for solar fuel synthesis by artificial photosynthesis; predicting the optical, electronic and redox properties of photocatalysts

Pierre Guiglion[1], Enrico Berardo[1,2], Cristina Butchosa[1], Milena C C Wobbe[1] and Martijn A Zwijnenburg[1]

[1] Department of Chemistry, University College London, 20 Gordon street, London WC1H 0AJ, UK
[2] Current address: Department of Chemistry, Imperial College London, South Kensington Campus, London SW7 2AZ, UK

E-mail: m.zwijnenburg@ucl.ac.uk

CrossMark

Abstract

In this mini-review, we discuss what insight computational modelling can provide into the working of photocatalysts for solar fuel synthesis and how calculations can be used to screen for new promising materials for photocatalytic water splitting and carbon dioxide reduction. We will extensively discuss the different relevant (material) properties and the computational approaches (DFT, TD-DFT, GW/BSE) available to model them. We illustrate this with examples from the literature, focussing on polymeric and nanoparticle photocatalysts. We finish with a perspective on the outstanding conceptual and computational challenges.

(Some figures may appear in colour only in the online journal)

Introduction

Motivated by concerns about the running out of fossil fuels and the role of CO_2 in climate change, the last twenty years have seen a worldwide research effort into solar fuel synthesis; the splitting of water to hydrogen [1–7] or reduction of CO_2 to hydrocarbons [8, 9] driven by the energy of solar light. Such solar fuels combine green credentials with a relatively easy incorporation into the existing infrastructure for fossil transport fuels and ease of storage relative to electricity.

Solar fuels can be synthesized in three different ways. Directly through artificial photosynthesis, the subject of this review, where absorption of light forms free charge carriers that drive *red-ox* reactions such as proton reduction or water oxidation. Directly, but via a thermochemical route, where concentrated light in the form of heat results in the direct disproportionation of water. Finally, solar fuels can also be synthesized indirectly via a combination of separate photovoltaics and electrolysis. All these approaches have in common that part of the energy of the light becomes absorbed in the solar fuel synthesis reaction products, allowing this otherwise endergonic reaction to take place.

Commonly, artificial photosynthesis is referred to as photocatalysis and the solid or molecule that mediates the processes
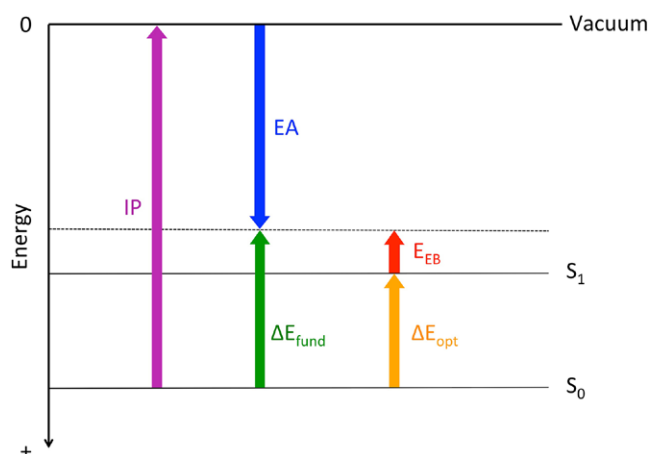
Figure 1. Illustration of the relevant energy gaps of a photocatalyst and their relationship with the vertical potentials. ΔE_{fund} is the fundamental gap (also referred to as the band, quasiparticle or transport gap) and equals the energy needed to make two non-interacting free charge carriers. ΔE_{opt} is the optical gap, the energy above which the photocatalyst will start to absorb light. E_{EB} is the exciton binding energy, the amount by which an electron-hole pair (exciton) is stabilised relative to free charge carriers due to their mutual electrostatic attraction. IP and EA, finally, are the vertical ionisation potential and electron affinity, the difference between which equals the fundamental gap.
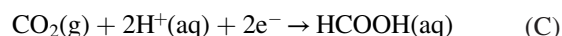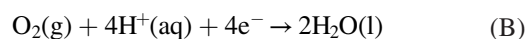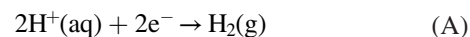
as a photocatalyst. While this choice of wording is in line with the IUPAC definition [10, 11] which states that photocatalysis is the '*change in the rate of a chemical reaction or its initiation under the action of ultraviolet, visible or infrared radiation in the presence of a substance—the photocatalyst—that absorbs light and is involved in the chemical transformation of the reaction partners*', this terminology can be confusing. No chemical catalysis, i.e. lowering of activation energies of reactions, necessarily takes place and a photocatalyst is very often not a catalyst in the chemical sense [12]. However, in the remainder of this review, we will follow the IUPAC definition and the de facto standard of the field and use photocatalysis and artificial photosynthesis interchangeably, as well as refer to the solid or molecule that acts as mediator as a photocatalyst. The latter, finally, can be dispersed in water [1, 2, 6] or take the form of one or both electrodes in a photoelectrochemical cell [4, 5, 7].

Different classes of materials have been reported in the literature to act as water oxidation, proton reduction and/or CO_2 reduction photocatalysts. The most well-known of these photocatalysts are the inorganic solids [1–3, 6], mostly oxides but also sulfides and selenides, the former including titanium dioxide [13–15], the quintessential photocatalyst. Perhaps less well-known, a range of supramolecular systems [16, 17] and even organic polymers [18–34] have also been reported to act as photocatalysts. In this mini-review we will discuss computational work on modelling such photocatalysts in terms of the relevant material properties and processes, as well as what we believe to be key aspects to consider when performing such calculations. We will focus predominantly on dispersed photocatalysts based on inorganic nanoparticles and polymers but will briefly touch on other systems where this makes sense.

Primer into the physical chemistry of artificial photosynthesis

When a material absorbs light of energy larger than the material's optical gap (see figure 1), electrons get excited from the top of the valence band (highest occupied molecular orbital in a molecular perspective) to the bottom of the conduction band (lowest unoccupied molecular orbital) and excitons, excited electron—hole pairs, are formed. These excitons can subsequently dissociate into free electrons and free holes, where 'free' refers to the fact that they are not bound together as excitons, through the supply of additional energy, the exciton binding energy. The latter can come in the form of thermal energy (thermal dissociation) or an electric field (field dissociation). These free electrons and holes can take part in interesting chemistry, e.g. reduce protons or oxidise water (see below), but also re-form excitons in a process commonly referred to as electron-hole recombination. Excitons, finally, can decay at any stage back to the ground state via either (photo)luminescence, emission of light, or via internal conversion, a dark non-radiative route, where the excess energy is dissipated in the form of phonons (atomic vibrations).

Solar fuel synthesis involves a combination of *red-ox* half reactions:

$$2H^+(aq) + 2e^- \rightarrow H_2(g) \qquad (A)$$

$$O_2(g) + 4H^+(aq) + 4e^- \rightarrow 2H_2O(l) \qquad (B)$$

$$CO_2(g) + 2H^+(aq) + 2e^- \rightarrow HCOOH(aq) \qquad (C)$$

Where *A–C* are all written in line with convention as reductions. Overall water splitting is a combination of half reactions *A* and *B*, with the latter running in the opposite direction to that written above, i.e. as an oxidation rather than a reduction. Similarly, the combination of half reactions *C* and *B* (again with half reaction *B* running in the opposite direction than written) describes the reduction of carbon dioxide to formic acid coupled with the oxidation of water, or alternatively put, the splitting of carbonic acid (H_2CO_3). Other possible CO_2 reduction products besides formic acid include carbon monoxide (2 electron reduction), formaldehyde (4 electron reduction), methanol (6 electron reduction) and methane (8 electron reduction).

Many experimental studies only investigate the ability of a material to drive one of the half reactions above, e.g. only hydrogen evolution. They use a sacrificial electron donor (SED) or sacrificial electron acceptor (SEA) to provide or accept electrons and to uncouple the studied half reaction from its natural counterpart. Examples of typical SEDs are methanol and triethylamine, while commonly used SEAs include Ag^+ and Ce^{4+} salts.

For a material to act as a photocatalyst for solar fuel synthesis, it should at least be thermodynamically able to provide electrons and holes to drive the combinations of *red-ox* half reactions discussed above. This can be analysed in terms of the potentials associated with the solar fuel synthesis half reactions and those associated with free electrons, holes and excitons in the photocatalyst [35, 36]. The half reactions for the free electrons, holes and excitons are:
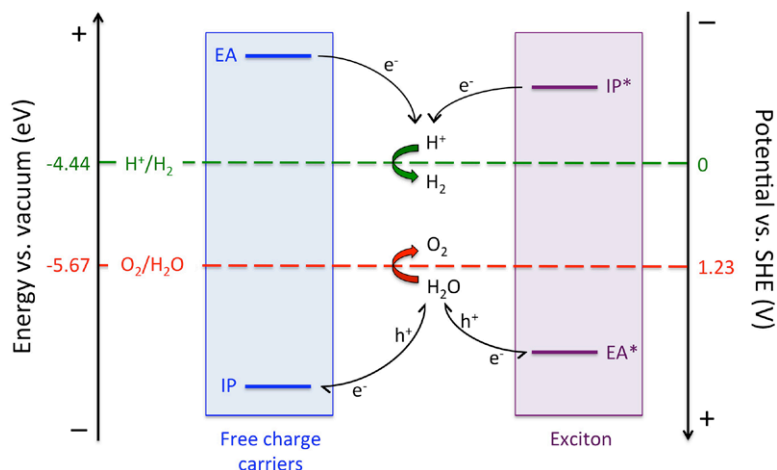
Figure 2. Scheme illustrating how the (standard) reduction potentials (IP, EA and EA* and IP*) of the ideal photocatalyst must straddle the proton reduction and water oxidation potentials (green and red broken lines respectively) in the case of water splitting.

$$P^+ + e^- \rightarrow P \qquad (D)$$

$$P + e^- \rightarrow P^- \qquad (E)$$

$$P^* + e^- \rightarrow P^- \qquad (F)$$

$$P^+ + e^- \rightarrow P^* \qquad (G)$$

where P is the neutral photocatalyst, P* the photocatalyst with an exciton localised on it, and P^+ and P^- the photocatalyst with a hole in its valence band and an excess electron in the conduction band respectively. The potential of half reaction D is often referred to as the ionisation potential (IP) or the valence band maximum (VBM), while the potential of half reaction E is commonly referred to as the electron affinity (EA) or the conduction band minimum (CBM). The exciton potentials F and G can in analogy be labelled as EA^* and IP^*. For the solar fuel synthesis to be exergonic in the presence of a photocatalyst, the IP/EA* and EA/IP* potentials should straddle the solar fuel synthesis half-reaction potentials (see figure 2). This constraint ensures that for both the oxidative and reductive parts of the overall solar fuel synthesis reaction, the net potential (IP/EA* − E_{Ox} and E_{Red} − EA/IP* respectively) is positive and that the associated Gibbs free energy change in both cases is negative. Moreover, energetic losses and kinetic barriers mean that the net potentials should not only be positive but also larger than approximately a couple of tenths of volts to achieve observable reaction rates.

Beyond the thermodynamic constraint on the photocatalyst potentials relative to those of solar fuel synthesis half reactions discussed above, there is also a thermodynamic constraint on the absolute magnitude of the photocatalyst's optical gap. The photocatalyst should naturally absorb a significant fraction of the solar spectrum but also have an optical gap big enough for the potentials to straddle the solar fuel synthesis half-reaction potentials: 1.23 V in the case of water splitting. In a single-phase photocatalyst for water splitting that means an optical gap of at least ~1.8 eV (~690 nm) and probably more, wasting the red and infrared part of the solar spectrum. Although for multi-phase photocatalysts coupled via a *red-ox* shuttle in a

Z-scheme [2, 6], this constraint is lifted and more of the sun's spectrum can be usefully absorbed.

Desired photocatalyst properties

Based on the discussion above, an ideal solar fuel synthesis photocatalyst should thus:

1. Absorb (visible) light.
2. Provide the thermodynamic driving force required for solar fuel synthesis.
3. Allow for facile exciton dissociation and electron-hole separation.
4. Have a low overpotential for the desired *red-ox* reactions.
5. Be stable under illumination and *red-ox* conditions.

The activity of a photocatalyst in solar fuel synthesis will be the product of and a compromise between all these materials' properties. For example, doping a material to reduce the optical gap and to allow more photons to be absorbed, probably also means a reduction in the thermodynamic driving force for solar fuel synthesis. The composite origin of activity also means that it is very hard to predict or explain the relative activity of different materials but modelling should be able to shed light on the more binary question of driving force, as well as provide insight on how the other parameters can be optimised.

Modelling

In the remainder we will discuss the current state of the art in modelling photocatalytic materials with reference, where possible, to recent literature. We will focus on modelling the optical gap, driving force, exciton dissociation, and required overpotential. The computational exploration of photocatalyst stability under operation conditions is, as far as we are aware, a relatively unexplored area of research, though the stability of inorganic photocatalysts in neutral water in the dark has been explored computationally [37, 38].

Optical gap

The optical gap, the energy above which light gets absorbed by a material, is perhaps the most often calculated property of a (potential) photocatalyst. Many such studies focus on how the optical gap of a material can be reduced so that the material absorbs more of the solar spectrum. For example, there is a multitude of papers considering the effect of doping on the optical gap of TiO_2 [39–50]. However, such papers generally suggest ways of improving the optical gap without considering the effect on the thermodynamic driving force for solar fuel production. Calculation of the optical gap and the overall optical absorption spectrum can also provide insight in the dominant structural elements of an (amorphous) photocatalyst, for example, to understand [36] the difference between differently prepared carbon nitride photocatalysts [21, 26].

In many cases, especially when studying periodic materials, authors approximate the optical gap with the density functional theory (DFT) Kohn-Sham (KS) gap: the energy difference between the highest energy occupied KS orbital and lowest energy virtual KS orbital. This approximation, hereafter referred to as KS-DFT, is computationally cheap; the KS orbital energies are anyway calculated as part of a ground state DFT calculation, and there is a good theoretical argument underlying it. In the case of calculations using pure density-dependent exchange-correlation (XC) functionals (i.e. LDA and GGA calculations), virtual orbitals feel the same *N-1 electron* KS potential as the occupied orbitals, in stark contrast to the case of Hartree–Fock theory (HFT), where the virtual and occupied orbitals experience *N* and *N-1 electron* potentials respectively. The presence of this stabilising hole (*N-1 electron*) potential in DFT, reminiscent of the potential that the excited electron component of an exciton would see, shifts the virtual orbitals downwards in energy relative to where they would lie in the case of HFT. As a result, the KS orbital gap behaves like the lowest excitation energy, the optical gap, rather than the energy to make a non-interacting free electron—free hole pair (the band or fundamental gap, see below), as it would be in HFT. There are reasons to be careful with applying the KS-DFT approximation in practice, however. Firstly, the approximation of the optical gap by the KS gap turns out to be problematic for solids, the case for which it is ironically most commonly used, with the KS gap typically being only 50–60% of the true optical gap. Secondly, even in the case of finite size systems, the situation is less clear when using hybrid XC functionals that mix pure density Kohn-Sham DFT with HFT (e.g. B3LYP [51–54], PBE0[55–57]). We would like to refer to a recent perspective by Baerends *et al* [58] for more details on these methodological issues. Finally, there is a question of terminology. In practice, even when using it as a proxy for the optical gap, the KS gap is often referred to as the band gap. The band gap (IP-EA, see figure 1, also referred to as the fundamental, transport or quasiparticle gap), however, is the energy required to make an unbound free electron and free hole pair, and hence equals the optical gap plus the exciton binding energy [59]. Use of band or fundamental gap as a synonym for optical gap suggests, probably erroneously, a negligible exciton binding energy.

Time-dependent DFT [60–62] (TD-DFT) and Bethe-Salpeter equation [63–65] (BSE) calculations do not suffer from this ambiguity as they explicitly describe excitations in terms of excitons. They also allow one to distinguish between excitations corresponding to different spin-states, e.g. singlet and triplet excitons, and the splitting between them. TD-DFT and BSE calculations are however no panacea. TD-DFT, just like ground state DFT, requires the choice of a XC functional and there are plenty of cases where commonly used XC functionals fail dramatically. A good example of the latter is the description of charge-transfer (CT) states involving under-coordinated surface atoms on the surface of inorganic nanoparticles [66–68], which requires use of range-separated XC functionals (e.g. CAM-B3LYP [69]) for accurate predictions. Vigilance, as well as benchmarking of TD-DFT results for small model systems against more accurate quantum chemistry calculations is therefore always advisable. BSE calculations are performed on top of Green's-function-based GW ionisation potential and electron affinity calculations [63, 70, 71], which are started from the eigenvalues and wavefunctions from a ground state DFT calculation. While self-consistent GW calculations are possible [72–76], most BSE calculations are performed on top of non self-consistent G_0W_0 or partially self-consistent GW_0 calculations and hence will show some dependence on the XC functional used in the underlying DFT calculation. GW calculation also requires testing for convergence in terms of the number of empty states to include, and the method and quality of frequency integration. Also, both TD-DFT and GW/BSE calculations are considerably more computationally expensive than ground state DFT calculations on the same system, although work on faster approximations and implementations of both methods is a subject of intense study. For organic systems and selected inorganic systems (e.g. ZnS [77, 78] but not TiO_2 for which they fail dramatically [79, 80]) approximate coupled-cluster methods, such as (RI-)CC2 [81, 82], can provide an attractive balance between accuracy and computational cost.

Finally, while the lowest energy singlet excitation, corresponding to the optical gap, is the most relevant excited state in the context of photocatalysis (P*) according to Kasha's principle [83], calculating the rest of the optical absorption spectrum of a photocatalyst by TD-DFT or GW/BSE is still a useful exercise. Such a calculation will give an idea of how strong a photocatalyst absorbs (visible) light, which is directly related to how many excitons are generated. It also allows one to weed out materials that have a small optical gap but do not strongly absorb light in the region above the optical gap, which, for example, can be a problem when using doping to optimise a material's optical properties.

Thermodynamic driving force

As discussed above, for a material to act as a photocatalyst for solar fuel synthesis, its IP/EA* and EA/IP* potentials should straddle the solar fuel synthesis half-reaction potentials. In the literature, three different conceptual approaches are used to calculate the photocatalyst potentials:
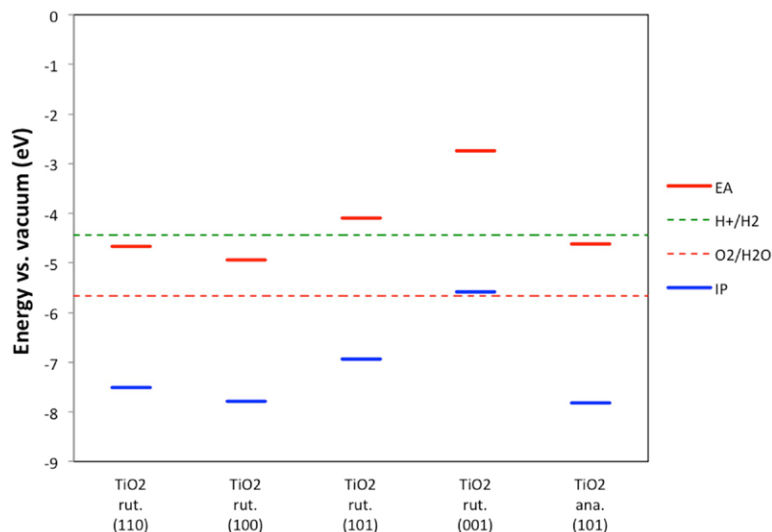
Figure 3. Illustration of the surface dependence of the potentials in the case of a crystalline inorganic photocatalyst. Data shown are the vertical potentials for different TiO_2 rutile and anatase surfaces predicted using GW by Stevanovic and co-workers [89].

I. Use of the KS orbital energies from ground state DFT; i.e. IP equals $-\varepsilon_{HOMO/VBM}$ and EA equals $-\varepsilon_{LUMO/CBM}$.

II. Explicit calculation of the vertical IP/EA* and EA/IP* potentials using Δ-SCF (TD-)DFT or GW/BSE.

III. Explicit calculation of the adiabatic IP/EA* and EA/IP* potentials using Δ-SCF (TD-)DFT or GW/BSE that include effect of self-trapping of free charge carriers and/or excitons.

Where approach *II* in the case of DFT reduces to approach *I* for infinitively extended materials modelled using periodic boundary conditions because the electron added or removed in the Δ-SCF calculation is shared out over an infinite number of atoms [84].

Approach *I*, KS-DFT, is probably the most commonly used in the literature but, just as the related approximation of the optical gap by the KS gap, is not without its problems. As discussed above, the difference between IP and EA equals the band or fundamental gap, which by definition is always larger than the optical gap. Now as the KS gap with LDA or GGA XC functionals is a good approximation to this optical gap for finite-size systems and even underestimates the true optical gap of infinitely extended solids (see discussion in the section above on predicting the optical gap), this must mean that the KS gap by definition always underestimates the true fundamental gap. As a result the IP and EA values determined from $-\varepsilon_{HOMO/VBM}$ and $-\varepsilon_{LUMO/CBM}$ must similarly lie away from their true values. Moreover, as most of the conceptual problems with mapping the KS gap onto either the optical or fundamental gap are related to the description of the virtual states, there are good reasons to believe that the majority of the discrepancy will lie with the EA value, i.e. that $-\varepsilon_{LUMO/CBM}$ will be considerably more negative than the true EA. Use of hybrid XC functionals will probably improve the results of approach *I* to a degree as it opens up the KS gap, bringing it closer to the true fundamental gap value. There is no guarantee that the amount of HF-like exchange (HFLE) required to achieve a good match to the true band

gap is the same for all systems, but at least for simple binary semiconductors this seems to be the case [85, 86]. In this context, we feel it is also opportune to mention the optimally tuned range-separated hybrid functional method of Kronik and co-workers [87, 88]. In their approach, the range-separation parameter of a range-separated XC functional is tuned, such that for a given system, the KS gap found with this XC functional is equal to the difference between the IP and EA potentials obtained in Δ-SCF calculations using the same XC functional. Finally, approach *I* cannot be used to calculate the IP* and EA* potentials.

While the use of $-\varepsilon_{HOMO/VBM}$ and $-\varepsilon_{LUMO/CBM}$ in approach *I* is problematic, due to the underestimation of the band gap by the KS gap, the DFT Δ-SCF and GW methods, underlying approaches *II* and *III*, allow for unambiguous calculations of the IP and EA potentials of a system. Moreover, the combination of these methods with TD-DFT and BSE calculations respectively allow also for the calculation of the excited state IP* and EA* potentials. Finally, the fact that the DFT Δ-SCF and GW methods allow for the explicit calculation of gradients for the states corresponding to IP and EA means that it is possible to study the effect of free charge carrier (self-)trapping on the potentials. This inclusion of nuclear relaxation in the calculation of the potentials is the only difference between approaches *II* and *III*. The Δ-SCF DFT/TD-DFT calculations will, just as TD-DFT calculations for the optical gap, show a dependence on the XC functional used, and benchmarking the results relative to available experimental data for (model) systems is always a good idea (cyclic voltammetry or photon electron spectroscopy data for potentials, as well as UV-VIS absorption and fluorescence data). Similarly, as discussed in the section on the optical gap, GW calculations can show a dependence on the XC functional used in the underlying DFT calculation.

Vertical potentials, based on approach *I* or *II*, are routinely reported in the literature [33, 89–99]. See the work of Stevanovic *et al* [89] for a nice illustration for the case of GW vertical potentials for the surfaces of typical crystalline
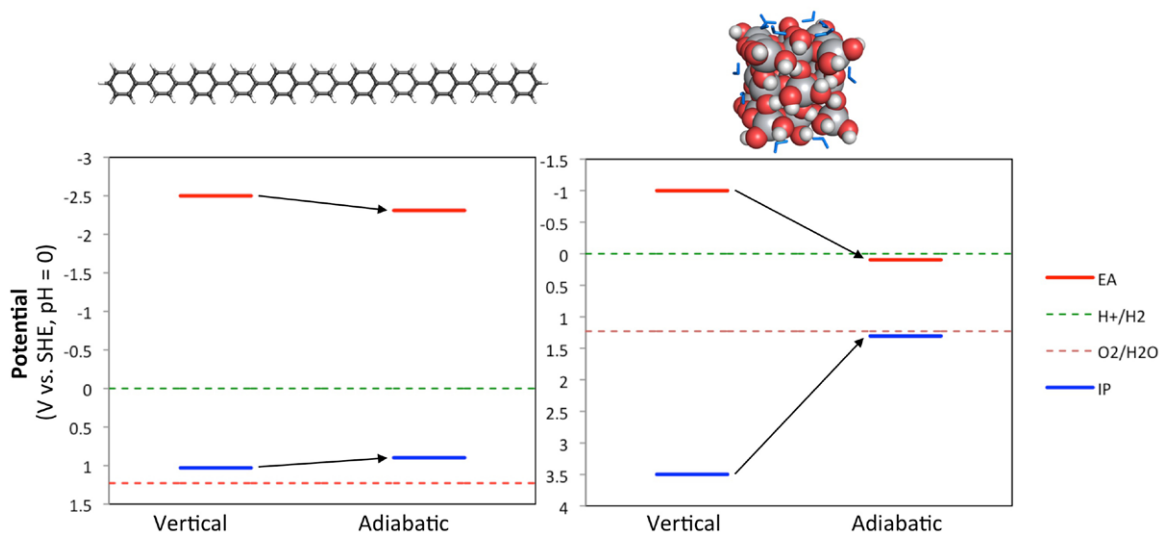
Figure 4. Comparison of the effect of self-trapping on the adiabatic potentials of an oligomeric photocatalyst (left, para-phenylene oligomer) and an inorganic nanoparticulate photocatalyst (right, hydrated and hydroxylated TiO_2 nanoparticle). Underlying data taken from [35] and [100] respectively.

photocatalysts, which also clearly illustrates that potentials are surface rather than bulk properties (see figure 3). Adiabatic potentials, which include the effect of self-trapping, however, are much less often calculated. We have reported adiabatic potentials for both polymer and inorganic nanoparticle photocatalysts [35, 36, 100], while others have studied the same potentials for nanoparticles in the context of dye-sensitized solar cells [101–103]. We are not aware of adiabatic calculations for slab models but there are a multitude of reports of computational studies of the trapping of free charge carriers and excitons in slabs of different materials [104–110]. The difference between vertical and adiabatic potentials appears small for conjugated polymeric systems and large(r) for inorganic nanoparticles (see figure 4), where the calculated trapping energies for nanoparticle also appear to be significantly larger than that of surfaces or the bulk of similar materials. The origin of the difference in trapping energies between inorganic nanoparticles and bulk surfaces is probably the enhanced flexibility of atoms on the surface of nanoparticles, while the difference between inorganic nanoparticles and conjugated polymers is probably related to the more delocalised electronic structure of the latter. Finally, calculations suggest, at least in the case of the trapping of excitons in nanoparticles, that there might be a landscape of different trapping minima [100, 111, 112], all associated with slightly different potentials [100].

The calculation of potentials requires the choice of a common reference for the energy of a free electron. For non-periodic calculations on finite-size systems, this is trivial as one can use the vacuum as a reference, i.e. an electron infinitely far away from the system that will have an energy of zero. In the case of periodic calculations, this reference choice is for obvious reasons not suitable. So instead, calculations on crystalline materials focus on slab models, infinitely extended in two dimensions and finite in size in the other direction, with vacuum gaps in between the slabs. Here, an electron at the centre of the vacuum gap is the reference state and the

difference in average macroscopic electrostatic potential between the centre of the slab and the centre of the vacuum gap is used to reference the potentials.

This brings us to modelling the effect of the environment in which the photocatalyst resides. Solar fuel synthesis generally takes place with the photocatalyst dispersed in water, while experiments involving SED typically take place in polar organic solvents with a relatively high dielectric permittivity, e.g. methanol. The presence of solvent will have some effect on the optical gap, mostly through the direct coordination of water or other solvent molecules to the surface, but the magnitude of the effect of solvent is generally much more pronounced in the case of potentials (see figure 5). There will be a shift in the vertical potentials due to both the presence of interface dipoles on the solvent—solid interface and the dielectric screening of free charges, where the latter effect will be most significant in the case of molecular systems, small nanoparticles or materials with a low relative dielectric permittivity. The adiabatic potentials will be further shifted by the influence of solvent on the (self-)trapping strength and localisation of both free charge carriers and excitons. In the case of calculations on slabs of crystalline materials with reasonably high relative dielectric permittivities (e.g. oxides), the effect on the vertical potentials can be treated using a semi-empirical rigid shift [89]. In contrast, calculations on small nanoparticles and cluster models of polymeric photocatalysts require the use of an implicit solvation model [113] that embeds the system in a dielectric continuum (see figure 5). The latter has to be combined with explicit hydration and/or hydroxylation of surface atoms for materials, such as oxides, on which water strongly physisorbs and/or chemisorbs [100–103]. Explicit hydration/hydroxylation, while making the calculations more realistic, also significantly adds to the complexity of the calculations. Not only will the number of atoms for the explicitly hydrated system be much larger than the unhydrated system, but many different minima are also likely to
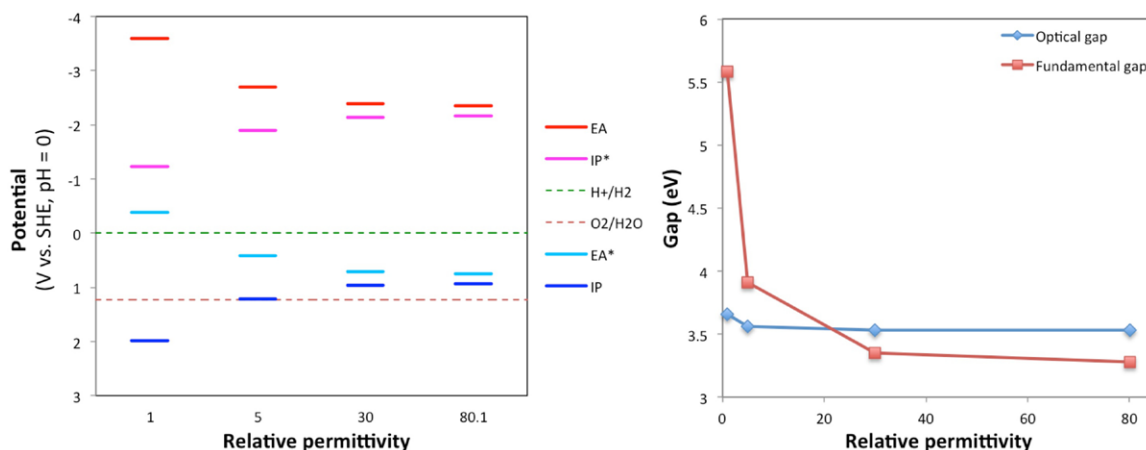
Figure 5. Effect of the environment on the adiabatic potentials (left) and optical and fundamental gap (right) of a para-phenylene oligomeric photocatalyst. Underlying data taken from reference 35, where the relative permittivity of the embedding dielectric continuum in the solvation model is varied between that of vacuum (1) and that of water (80.1).

exist, only differing in the arrangement of the water molecules and hydroxyl groups. Adiabatic calculations probably require at least hydration and/or hydroxylation of surface atoms as the presence of water molecules on the surface is likely to change the (self-)trapping location and strength of both free charge carriers and excitons. Finally, when comparing to experimental (electrochemical) data, it is important to be aware that away from a material's point of zero charge (PZC), its surface will be (de)protonated. As a result, the reported experimental flatband potentials for such materials contain a contribution due to the potential drop over the Helmholtz layer due to the specific adsorption of OH^- or H^+ on the surface. This is especially relevant when comparing to experimental potentials tabulated at standard conditions, e.g. pH 0 or pH 1, values that are much lower and higher respectively than the PZC of many (potential) photocatalyst materials. Similarly, adsorption of other ions from solution or the intentional modification of the surface with adsorbants with a large dipole moment [114] will shift the photocatalyst potentials relative to those of the solution *red-ox* reactions and can be used to engineer the potentials of a photocatalyst beyond what is possible by changing the bulk chemical composition alone. Please see work by Butler *et al* [115] and Stevanovic *et al* [89] on how this influences the comparison between computational prediction and experimental measurement.

The relative potentials of all the solution *red-ox* reactions, except the proton reduction half reaction *A*, can either be taken from experiment or recalculated using a computational setup similar to that used to calculate the photocatalyst potentials. The absolute potential half reaction *A*, however, is normally always taken from experiment (4.44 eV) [116] as calculating it *a priori* is fraught with difficulties [117–119], even if Wu *et al* [120] are able to make good predictions of the relative difference between potential *A* and the CBM of different materials without the need of recourse to experimental data. The relative potentials of the solution *red-ox* reactions, as well as those of the photocatalyst, can be calculated using the standard

relationship ($\Delta G^0 = -nFE^0$) between the Gibbs free energy (ΔG^0) and potential (E^0). The effect of pH on the solution potentials, finally, can be modelled using the Nernst equation.

Exciton dissociation and electron-hole separation

While the kinetics of elementary steps of the *red-ox* half reactions are presumably similar when using a material as photocatalyst or as an electrode in electrolysis, the contributions to kinetics arising from the finite lifetime of excitons and free charge carriers is probably unique to photocatalysis. Moreover, there are good reasons to believe that this contribution is critical for a catalyst to be able, or not, to drive particular solar fuel synthesis half reactions, see below.

To optimally make use of all light absorbed, especially for materials with long penetration depths for light (i.e. weak light absorbers), exciton dissociation is crucial. The exciton binding energy, which governs how easy it is to break up an exciton, is hence a key parameter to minimise. When using method combinations that allow for the explicit calculation of both the optical and fundamental gaps ((TD-)DFT, GW/BSE) the exciton binding energy can be obtained trivially. For methods that do not and only allow for the calculation of the fundamental gap (KS-DFT), the exciton binding energy can be obtained via semi-empirical models. For example, Sautet and co-workers [86] use a semi-empirical Wannier exciton model in combination with DFT calculated dielectric permittivity and electron and hole effective mass values to estimate exciton binding energies. They find that the screened hybrid XC functional HSE06 [121,122] gives both good exciton binding energy and fundamental gap values for group 14 elements and simple binary inorganic semiconductors.

In small nanoparticles and/or materials in which the exciton binding energy is too large for thermal dissociation, excitons have to diffuse to the water-photocatalyst interface and dissociate there, see figure 6. In this scenario, one free charge carrier remains in the photocatalyst while the other goes into solution; i.e. is consumed by a solution *red-ox*
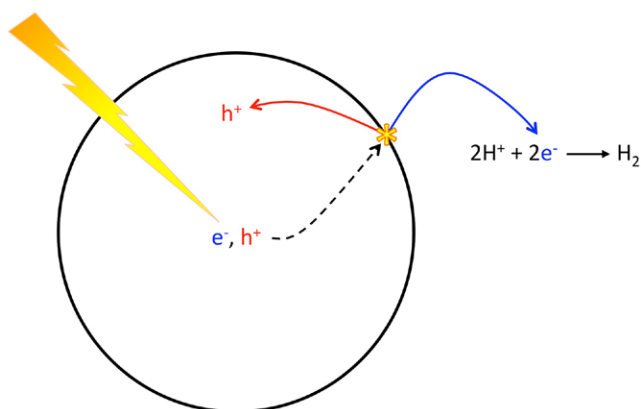
Figure 6. Illustration of exciton dissociation at the surface of a nanoparticle for the case where the electron of the exciton goes into solution, where it drives proton reduction, while the hole remains on the particle.

reaction. For example, an exciton can dissociate on a photocatalyst-solution interface with the free hole remaining on the photocatalyst and the electron reducing a proton (half reaction *A*) or taking part in a side-reaction like the formation of the superoxide radical (O_2^-) from dissolved molecular oxygen. From a computational point of view, this interface exciton dissociation is described by a combination of the photocatalyst potentials that involve the exciton (IP* and EA*, half reactions *F* and *G*) and the relevant solution *red-ox* potentials. If IP* is more negative than the potential of a solution *red-ox* reaction that accepts electrons or EA* more positive than the potential of a solution *red-ox* reaction that donates electrons, exciton dissociation on the photocatalyst-solution interface can take place. Calculations suggest that this mechanism of exciton dissociation is the main origin of free charge carriers and photocatalytic activity in polymers (polyphenylene, conjugated microporous polymers, carbon nitride) [33, 35, 36], which are predicted to have exciton binding energies of tenths of electronvolt.

Excitons can also dissociate on interfaces other than that between the photocatalyst and solution. Many photocatalysts are comprised of more than one material or phase and the exciton can dissociate on the interface between two of these phases/materials. The formation of heterostructures can be intentional, as for example in the carbon nitride—carbon nanodots [34] and carbon nitride—polypyrrole [29] systems, or an unintentional side-effect of the material's preparation, as in for example the often used Degussa P25 titanium dioxide, which is a mixture of the anatase and rutile phases. Presence of these heterostructures can have a very significant effect on the photocatalytic activity. For example, the carbon nitride heterostructures highlighted above are reported to be active for overall water splitting while carbon nitride on its own is not. From a computational point of view, the exciton dissociation at the interface between the different components of a heterostructure can be understood in terms of the alignment between the KS/GW levels (in the case of KS levels with the shortcomings discussed above) or potentials on either side of the interface. Scanlon and co-workers [123] performed

such calculation to shed light on the controversial alignment between the levels in anatase and rutile titanium dioxide [124–127], while we considered [36] what happens at the interface between carbon nitride and polypyrrole to understand the overall water splitting activity of the heterostructure discussed above. One complicating factor is that in the case of doped materials, the Fermi level on both sides of the interface has to align, changing in the process the relative alignment of the levels/potentials, as well as leading to the formation of an electrostatic potential over the interface.

The lifetime of excitons before dissociation and how this is influenced by the photocatalyst structure (e.g. presence of defects), finally, can be approximated when using TD-DFT, and when neglecting radiationless de-excitation via internal conversion, from the oscillator strength of the corresponding excitation via Einstein's equation for spontaneous emission. Calculation of the dark contribution to the exciton lifetime and of (exciton) dynamics in general requires non-adiabatic dynamics calculations, which explicitly take into account the coupling between the different energy surfaces [128–136]. Such calculations, however, are for the moment rather far from routine. The same holds for calculations that aim to model the mobility of free charge carriers [137–143], which is a crucial property for good photoelectrodes but less relevant for polymeric and nanoparticulate systems where exciton dissociation occurs on the surface, and for calculations that explicitly study the electron/hole transfer between different sub-components of the photocatalyst and the photocatalyst and solution/surface species [99, 144].

Required overpotential

Computational work on predicting the required overpotential for desired *red-ox* reactions mostly takes place in the context of computational electrochemistry [145–149]. Here the overpotential required for a half reaction (e.g. *A* or *B*) to take place is analysed in terms of the thermodynamic potentials of the series of elementary reactions that underlie it. An ideal material would bind all the intermediates (e.g. HO*, O* and HOO* in the case of water oxidation, where the asterisk signifies chemisorption on the surface) equally strong and if that is not the case an additional potential has to be overcome for the overall half reaction to occur. The difference between the potential of the least favourable elementary reaction and the potential of the overall half reaction equals the thermodynamic overpotential [146]. While this approach does not explicitly take the activation energies of the different elementary reactions into account, it is likely that the best materials in terms of thermodynamic overpotential are also the materials with the lowest and thus most favourable activation energies. This arises from the fact that the activation energy of an elementary step is often directly related to the thermodynamic driving force for the same step through a Brönsted-Evans-Polyani relationship. An example of the application of this approach to a photocatalyst is the recent work of Wirth and co-workers on the required overpotential for water oxidation on graphitic carbon nitride [150].

Perspective

Computational chemistry calculations can make valuable predictions of photocatalyst properties that underlie their activity in solar fuel synthesis. However, predictions of the (relative) photocatalytic activity of a material largely remain out of reach, at least for the moment, due to the fact that it depends on a mixture of materials' properties, where the relative importance of each property to the activity probably varies from material to material. As a result, it makes sense to focus on answering questions for which one of the properties is likely to be the dominant factor, for example, whether the lack of experimental evidence for water oxidation activity of a photocatalyst is likely to be due to thermodynamic or kinetic factors [35, 36].

Another clear application of computational modelling in this context is to rapidly screen for potential photocatalysts [92–95]. Both in the case of inorganic and polymeric photocatalysts, the possible chemical space is enormous. For example, for inorganic photocatalysts, most work until now has only focussed on binary and ternary materials. Experimental screening of this chemical space is a daunting task, mostly because of the large synthetic effort required. Computational screening to generate promising leads and narrow the search space for a more focussed subsequent experimental exploration is therefore an attractive proposition, even if one cannot necessarily predict the exact relative ordering of photocatalytic activities.

The biggest challenge, as often in computational chemistry, is striking the correct balance between computational cost, the ability to consistently calculate all the desired properties, and accuracy. KS-DFT, for example, is relatively computationally inexpensive and with a well-chosen hybrid XC functional is likely to predict band gap values of reasonable accuracy, ignoring the conceptual issues raised above, but requires use of an additional semi-empirical model to predict the exciton binding energy and optical gap. Moreover, KS-DFT does not allow one to consider the effect of (self-)trapping and calculate adiabatic potentials. (TD-)DFT and GW/BSE calculations, in principle, allow access to any desired property but at the expense of increased cost of calculations. The latter especially becomes an issue when studying the effect of particle-size on the photocatalyst properties, requiring calculations involving hundreds of atoms. In practice, the optimal computational approach, in terms of the balance between accuracy, speed and the ability to calculate desired quantities, will depend on the focus of the study. For example, when screening thousands of potential photocatalysts, KS-DFT is probably the only tractable option. In the end the most important thing, as often, is to be aware of what a method is meant to calculate, its (conceptual) shortfalls, and to benchmark, where possible, to experimental data.

Acknowledgments

References

[1] Kudo A and Miseki Y 2009 *Chem. Soc. Rev.* **38** 253
[2] Maeda K and Domen K 2010 *J. Phys. Chem. Lett.* **1** 2655
[3] Osterloh F E 2013 *Chem. Soc. Rev.* **42** 2294
[4] Joya K S, Joya Y F, Ocakoglu K and van de Krol R 2013 *Angew. Chem. Int. Ed.* **52** 10426
[5] Cowan A J and Durrant J R 2013 *Chem. Soc. Rev.* **42** 2281
[6] Hisatomi T, Kubota J and Domen K 2014 *Chem. Soc. Rev.* **43** 7520
[7] Li J and Wu N 2015 *Catal. Sci. Technol.* **5** 1360
[8] Roy S C, Varghese O K, Paulose M and Grimes C A 2010 *ACS Nano* **4** 1259
[9] Habisreutinger S N, Schmidt-Mende L and Stolarczyk J K 2013 *Angew. Chem. Int. Ed.* **52** 7372
[10] Braslavsky S E 2007 *Pure Appl. Chem.* **79** 293
[11] 2015 *IUPAC Gold Book* http://goldbook.iupac.org/
[12] Ohtani B 2008 *Chem. Lett.* **37** 216
[13] Sato S and White J M 1980 *Chem. Phys. Lett.* **72** 83
[14] Maeda K 2013 *Chem. Commun.* **49** 8404
[15] Maeda K 2014 *Catal. Sci. Technol.* **4** 1949
[16] Wasielewski M R 2009 *Acc. Chem. Res.* **42** 1910
[17] Gust D, Moore T A and Moore A L 2009 *Acc. Chem. Res.* **42** 1890
[18] Yanagida S, Kabumoto A, Mizumoto K, Pac C and Yoshino K 1985 *J. Chem. Soc., Chem. Commun.* 474
[19] Matsuoka S, Kohzuki T, Kuwana Y, Nakamura A and Yanagida S 1992 *J. Chem. Soc. Perkin Trans. 2* (doi: 10.1039/p29920000679)
[20] Maruyama T and Yamamoto T 1997 *J. Phys. Chem.* B **101** 3806
[21] Wang X C, Maeda K, Thomas A, Takanabe K, Xin G, Carlsson J M, Domen K and Antonietti M 2009 *Nat. Mater.* **8** 76
[22] Schwab M G, Hamburger M, Feng X, Shu J, Spiess H W, Wang X, Antonietti M and Müllen K 2010 *Chem. Commun.* **46** 8932
[23] Zhang Z, Long J, Yang L, Chen W, Dai W, Fu X and Wang X 2011 *Chem. Sci.* **2** 1826
[24] Chu S, Wang Y, Guo Y, Zhou P, Yu H, Luo L, Kong F and Zou Z 2012 *J. Mater. Chem.* **22** 15519
[25] Cui Y, Ding Z, Fu X and Wang X 2012 *Angew. Chem. Int. Ed.* **51** 11814
[26] Jorge A B, Martin D J, Dhanoa M T S, Rahman A S, Makwana N, Tang J W, Sella A, Cora F, Firth S, Darr J A and McMillan P F 2013 *J. Phys. Chem.* C **117** 7178
[27] Schwinghammer K, Tuffy B, Mesch M B, Wirnhier E, Martineau C, Taulelle F, Schnick W, Senker J and Lotsch B V 2013 *Angew. Chem. Int. Ed.* **52** 2435
[28] Ge L, Han C, Xiao X, Guo L and Li Y 2013 *Mater. Res. Bull.* **48** 3919
[29] Sui Y, Liu J, Zhang Y, Tian X and Chen W 2013 *Nanoscale* **5** 9150
[30] Kailasam K, Schmidt J, Bildirir H, Zhang G, Blechert S, Wang X and Thomas A 2013 *Macromol. Rapid Commun.* **34** 1008
[31] Hong Z, Shen B, Chen Y, Lin B and Gao B 2013 *J. Mater. Chem.* A **1** 11754
[32] Martin D J, Qiu K, Shevlin S A, Handoko A D, Chen X, Guo Z and Tang J 2014 *Angew. Chem. Int. Ed.* **53** 9240
[33] Sprick R S, Jiang J-X, Bonillo B, Ren S, Ratvijitvech T, Guiglion P, Zwijnenburg M A, Adams D J and Cooper A I 2015 *J. Am. Chem. Soc.* **137** 3265

[34] Liu J, Liu Y, Liu N, Han Y, Zhang X, Huang H, Lifshitz Y, Lee S-T, Zhong J and Kang Z 2015 *Science* **347** 970
[35] Guiglion P, Butchosa C and Zwijnenburg M 2014 *J. Mater. Chem.* A **2** 11996
[36] Butchosa C, Guiglion P and Zwijnenburg M A 2014 *J. Phys. Chem.* C **118** 24833
[37] Zhuang H L and Hennig R G 2013 *Chem. Mater.* **25** 3232
[38] Zhuang H L and Hennig R G 2013 *J. Phys. Chem.* C **117** 20440
[39] Di Valentin C, Pacchioni G and Selloni A 2005 *Chem. Mater.* **17** 6656
[40] Yang K, Dai Y, Huang B and Han S 2006 *J. Phys. Chem.* B **110** 24011
[41] Di Valentin C, Finazzi E, Pacchioni G, Selloni A, Livraghi S, Paganini M C and Giamello E 2007 *Chem. Phys.* **339** 44
[42] Yang K, Dai Y, Huang B and Whangbo M-H 2008 *Chem. Mater.* **20** 6528
[43] Finazzi E, Di Valentin C and Pacchioni G 2009 *J. Phys. Chem.* C **113** 220
[44] Shevlin S A and Woodley S M 2010 *J. Phys. Chem.* C **114** 17333
[45] Li H, Lei Y, Tu R, Zheng Y, Pan C and Xiao W 2011 *Phys. Status Solidi* B **248** 1665
[46] Tosoni S, Fernandez Hevia D, González Díaz Ó and Illas F 2012 *J. Phys. Chem. Lett.* **3** 2269
[47] Yu J, Zhou P and Li Q 2013 *Phys. Chem. Chem. Phys.* **15** 12040
[48] Di Valentin C and Pacchioni G 2013 *Catal. Today* **206** 12
[49] Ortega Y, Lamiel-Garcia O, Hevia D F, Tosoni S, Oviedo J, San-Miguel M A and Illas F 2013 *Surf. Sci.* **618** 154
[50] Di Valentin C and Pacchioni G 2014 *Acc. Chem. Res.* **47** 3233
[51] Vosko S H, Wilk L and Nusair M 1980 *Can. J. Phys.* **58** 1200
[52] Lee C, Yang W and Parr R G 1988 *Phys. Rev.* B **37** 785
[53] Becke A D 1993 *J. Chem. Phys.* **98** 5648
[54] Stephens P J, Devlin F J, Chabalowski C F and Frisch M J 1994 *J. Phys. Chem.* **98** 11623
[55] Perdew J P, Burke K and Ernzerhof M 1996 *Phys. Rev. Lett.* **77** 3865
[56] Perdew J P, Burke K and Ernzerhof M 1997 *Phys. Rev. Lett.* **78** 1396
[57] Adamo C and Barone V 1999 *J. Chem. Phys.* **110** 6158
[58] Baerends E J, Gritsenko O V and van Meer R 2013 *Phys. Chem. Chem. Phys.* **15** 16408
[59] Brédas J-L 2014 *Mater. Horiz.* **1** 17
[60] Hohenberg P and Kohn W 1964 *Phys. Rev.* B **136** 864
[61] Kohn W and Sham L J 1965 *Phys. Rev.* A **140** 1133
[62] Runge E and Gross E K U 1984 *Phys. Rev. Lett.* **52** 997
[63] Onida G, Reining L and Rubio A 2002 *Rev. Mod. Phys.* **74** 601
[64] Faber C, Boulanger P, Attaccalite C, Duchemin I and Blase X 2014 *Phil. Trans. R. Soc.* A **372** 20130271
[65] Jacquemin D, Duchemin I and Blase X 2015 *J. Chem. Theory Comput.* **11** 3290
[66] Berardo E, Hu H-S, Shevlin S A, Woodley S M, Kowalski K and Zwijnenburg M A 2014 *J. Chem. Theory Comput.* **10** 1189
[67] Berardo E, Hu H-S, van Dam H J J, Shevlin S A, Woodley S M, Kowalski K and Zwijnenburg M A 2014 *J. Chem. Theory Comput.* **10** 5538
[68] Wobbe M C C, Kerridge A and Zwijnenburg M A 2014 *Phys. Chem. Chem. Phys.* **16** 22052
[69] Yanai T, Tew D P and Handy N C 2004 *Chem. Phys. Lett.* **393** 51
[70] Aryasetiawan F and Gunnarsson O 1998 *Rep. Prog. Phys.* **61** 237
[71] Lars H 1999 *J. Phys.: Condens. Matter* **11** R489
[72] van Schilfgaarde M, Kotani T and Faleev S 2006 *Phys. Rev. Lett.* **96** 226402
[73] Shishkin M, Marsman M and Kresse G 2007 *Phys. Rev. Lett.* **99** 246403
[74] Shishkin M and Kresse G 2007 *Phys. Rev.* B **75** 235102
[75] Rostgaard C, Jacobsen K W and Thygesen K S 2010 *Phys. Rev.* B **81** 085103
[76] Caruso F, Rinke P, Ren X, Scheffler M and Rubio A 2012 *Phys. Rev.* B **86** 081102
[77] Zwijnenburg M A, Sousa C, Illas F and Bromley S T 2011 *J. Chem. Phys.* **134** 064511
[78] Azpiroz J M, Ugalde J M and Infante I 2014 *J. Chem. Theory Comput.* **10** 76
[79] Taylor D J and Paterson M J 2010 *J. Chem. Phys.* **133** 204302
[80] Berardo E, Hu H-S, Kowalski K and Zwijnenburg M A 2013 *J. Chem. Phys.* **139** 064313
[81] Christiansen O, Koch H and Jørgensen P 1995 *Chem. Phys. Lett.* **243** 409
[82] Hattig C and Weigend F 2000 *J. Chem. Phys.* **113** 5154
[83] Kasha M 1950 *Discuss. Faraday Soc.* **9** 14
[84] Sham L J and Schlüter M 1983 *Phys. Rev. Lett.* **51** 1888
[85] Heyd J and Scuseria G E 2004 *J. Chem. Phys.* **121** 1187
[86] Bahers T L, Rérat M and Sautet P 2014 *J. Phys. Chem.* C **118** 5997
[87] Refaely-Abramson S, Baer R and Kronik L 2011 *Phys. Rev.* B **84** 075144
[88] Kronik L, Stein T, Refaely-Abramson S and Baer R 2012 *J. Chem. Theory Comput.* **8** 1515
[89] Stevanovic V, Lany S, Ginley D S, Tumas W and Zunger A 2014 *Phys. Chem. Chem. Phys.* **16** 3706
[90] Toroker M C, Kanan D K, Alidoust N, Isseroff L Y, Liao P and Carter E A 2011 *Phys. Chem. Chem. Phys.* **13** 16644
[91] Kanan D K and Carter E A 2012 *J. Phys. Chem.* C **116** 9876
[92] Castelli I E, Olsen T, Datta S, Landis D D, Dahl S, Thygesen K S and Jacobsen K W 2012 *Energy Environ. Sci.* **5** 5814
[93] Castelli I E, Landis D D, Thygesen K S, Dahl S, Chorkendorff I, Jaramillo T F and Jacobsen K W 2012 *Energy Environ. Sci.* **5** 9034
[94] Wu Y and Ceder G 2013 *J. Phys. Chem.* C **117** 24710
[95] Wu Y, Lazic P, Hautier G, Persson K and Ceder G 2013 *Energy Environ. Sci.* **6** 157
[96] Zhang H, Zuo X, Tang H, Li G and Zhou Z 2015 *Phys. Chem. Chem. Phys.* **17** 6280
[97] Jiang X, Wang P and Zhao J 2015 *J. Mater. Chem.* A **3** 7750
[98] Buckeridge J, Butler K T, Catlow C R A, Logsdail A J, Scanlon D O, Shevlin S A, Woodley S M, Sokol A A and Walsh A 2015 *Chem. Mater.* **27** 3844
[99] Pastore M and De Angelis F 2015 *J. Am. Chem. Soc.* **137** 5798
[100] Berardo E and Zwijnenburg M A 2015 *J. Phys. Chem.* C **119** 13384
[101] Zhang J, Hughes T F, Steigerwald M, Brus L and Friesner R A 2012 *J. Am. Chem. Soc.* **134** 12028
[102] Zhang J, Steigerwald M, Brus L and Friesner R A 2014 *Nano Lett.* **14** 1785
[103] Nunzi F, Agrawal S, Selloni A and De Angelis F 2015 *J. Chem. Theory Comput.* **11** 635
[104] Stoneham A M, Gavartin J, Shluger A L, Kimmel A V, Ramo D M, Rønnow H M, Aeppli G and Renner C 2007 *J. Phys.: Conden. Matter* **19** 255208
[105] Mattioli G, Alippi P, Filippone F, Caminiti R and Amore Bonapasta A 2010 *J. Phys. Chem.* C **114** 21694
[106] McKenna K P and Shluger A L 2011 *Proc. R. Soc.* A **467** 2043
[107] Di Valentin C and Selloni A 2011 *J. Phys. Chem. Lett.* **2** 2223
[108] Varley J B, Janotti A, Franchini C and Van de Walle C G 2012 *Phys. Rev.* B **85** 081109
[109] Zawadzki P, Laursen A B, Jacobsen K W, Dahl S and Rossmeisl J 2012 *Energy Environ. Sci.* **5** 9866

[110] Spreafico C and VandeVondele J 2014 *Phys. Chem. Chem. Phys.* **16** 26144
[111] Zwijnenburg M A 2012 *Nanoscale* **4** 3711
[112] Zwijnenburg M A 2013 *Phys. Chem. Chem. Phys.* **15** 11119
[113] Tomasi J, Mennucci B and Cammi R 2005 *Chem. Rev.* **105** 2999
[114] MacLeod B A, Steirer K X, Young J L, Koldemir U, Sellinger A, Turner J A, Deutsch T G and Olson D C 2015 *ACS Appl. Mater. Interfaces* **7** 11346
[115] Butler M A and Ginley D S 1978 *J. Electrochem. Soc.* **125** 228
[116] Trasatti S 1986 *J. Electroanal. Chem. Interfacial Electrochem.* **209** 417
[117] Zhan C-G and Dixon D A 2001 *J. Phys. Chem.* A **105** 11534
[118] Bryantsev V S, Diallo M S and Goddard W A III 2008 *J. Phys. Chem.* B **112** 9709
[119] Cheng J and Sprik M 2010 *Phys. Rev.* B **82** 081406
[120] Wu Y, Chan M K Y and Ceder G 2011 *Phys. Rev.* B **83** 235301
[121] Heyd J, Scuseria G E and Ernzerhof M 2003 *J. Chem. Phys.* **118** 8207
[122] Heyd J, Scuseria G E and Ernzerhof M 2006 *J. Chem. Phys.* **124** 219906
[123] Scanlon D O *et al* 2013 *Nat. Mater.* **12** 798
[124] Li G and Gray K A 2007 *Chem. Phys.* **339** 173
[125] Kumar S G and Devi L G 2011 *J. Phys. Chem.* A **115** 13211
[126] Kapilashrami M, Zhang Y, Liu Y-S, Hagfeldt A and Guo J 2014 *Chem. Rev.* **114** 9662
[127] Quesada-Cabrera R, Sotelo-Vazquez C, Bear J C, Darr J A and Parkin I P 2014 *Adv. Mater. Interfaces* **1** 1400069
[128] Duncan W R, Craig C F and Prezhdo O V 2007 *J. Am. Chem. Soc.* **129** 8528
[129] Tapavicza E, Tavernelli I, Rothlisberger U, Filippi C and Casida M E 2008 *J. Chem. Phys.* **129** 124108
[130] Fischer S A, Duncan W R and Prezhdo O V 2009 *J. Am. Chem. Soc.* **131** 15483
[131] Long R and Prezhdo O V 2011 *J. Am. Chem. Soc.* **133** 19240
[132] Tapavicza E, Meyer A M and Furche F 2011 *Phys. Chem. Chem. Phys.* **13** 20986
[133] Long R, English N J and Prezhdo O V 2012 *J. Am. Chem. Soc.* **134** 14238
[134] Long R, English N J and Prezhdo O V 2013 *J. Am. Chem. Soc.* **135** 18892
[135] Akimov A V and Prezhdo O V 2013 *J. Chem. Theory Comput.* **9** 4959
[136] Tapavicza E, Bellchambers G D, Vincent J C and Furche F 2013 *Phys. Chem. Chem. Phys.* **15** 18336
[137] Deskins N A and Dupuis M 2007 *Phys. Rev.* B **75** 195212
[138] Deskins N A and Dupuis M 2009 *J. Phys. Chem.* C **113** 346
[139] Liao P, Toroker M C and Carter E A 2011 *Nano Lett.* **11** 1775
[140] Kronawitter C X *et al* 2014 *Energy Environ. Sci.* **7** 3100
[141] Adelstein N, Neaton J B, Asta M and De Jonghe L C 2014 *Phys. Rev.* B **89** 245115
[142] Peng H, Ndione P F, Ginley D S, Zakutayev A and Lany S 2015 *Phys. Rev. X* **5** 021016
[143] Kweon K E, Hwang G S, Kim J, Kim S and Kim S 2015 *Phys. Chem. Chem. Phys.* **17** 256
[144] Akimov A V, Neukirch A J and Prezhdo O V 2013 *Chem. Rev.* **113** 4496
[145] Rossmeisl J, Qu Z W, Zhu H, Kroes G J and Nørskov J K 2007 *J. Electroanal. Chem.* **607** 83
[146] Koper M T M and Bouwman E 2010 *Angew. Chem. Int. Ed.* **49** 3723
[147] Man I C, Su H-Y, Calle-Vallejo F, Hansen H A, Martínez J I, Inoglu N G, Kitchin J, Jaramillo T F, Nørskov J K and Rossmeisl J 2011 *ChemCatChem* **3** 1159
[148] Calle-Vallejo F and Koper M T M 2012 *Electrochim. Acta* **84** 3
[149] Halck N B, Petrykin V, Krtil P and Rossmeisl J 2014 *Phys. Chem. Chem. Phys.* **16** 13682
[150] Wirth J, Neumann R, Antonietti M and Saalfrank P 2014 *Phys. Chem. Chem. Phys.* **16** 15917